

Searching for Possible Exoplanet Transits from BRITE Data through a Machine Learning Technique

Li-Chin Yeh¹ and Ing-Guey Jiang²

¹*Institute of Computational and Modeling Science,
National Tsing Hua University, Hsin-Chu, Taiwan*

²*Department of Physics and Institute of Astronomy,
National Tsing Hua University, Hsin-Chu, Taiwan*

lichinyeh@mx.nthu.edu.tw, jiang@phys.nthu.edu.tw

ABSTRACT

The photometric light curves of BRITE satellites were examined through a machine learning technique to investigate whether there are possible exoplanets moving around nearby bright stars. Focusing on different transit periods, several convolutional neural networks were constructed to search for transit candidates. The convolutional neural networks were trained with synthetic transit signals combined with BRITE light curves until the accuracy rate was higher than 99.7 %. Our method could efficiently lead to a small number of possible transit candidates. Among these ten candidates, two of them, HD37465, and HD186882 systems, were followed up through future observations with a higher priority. The codes of convolutional neural networks employed in this study are publicly available at <http://www.phys.nthu.edu.tw/~jiang/BRITE2020Yeh.JiangCNN.tar.gz>.

1. Introduction

The discoveries of extra-solar planets (exoplanets) have significantly impacted astronomical sciences and advanced our understanding of the universe. Among many detection techniques, the transit method became one of the major players after the Kepler Space Telescope detected thousands of exoplanet candidates (Borucki et al. 2011). The light curves obtained through the Kepler Space Telescope (Kepler light curves hereafter) have been released. These valuable data were further examined and led to many potentially useful results. For example, Xie (2013) did the transit timing analysis on Kepler light curves and found several near-resonance planetary pairs. Ioannidis et al. (2014) further analyzed the light curves of Kepler-210 and detected two short-period planets. Later, Sun et al. (2019) employed the

light-curve data of the Kepler-411 system and revealed the existence of additional planets. Thus, it is now suggested there are four planets in the Kepler-411 system. Recently, Socia et al. (2020) discovered from Kepler light curves, a new Neptune-sized transiting circumbinary planet.

To monitor more stars, the telescopes of survey projects need to be capable of measuring the photometry of faint stars with larger apparent magnitude. The Kepler Space Telescope can monitor stars with an apparent magnitude around $V = 11 \sim 14$. Additionally, the CoRoT project focuses on stars with an apparent magnitude around $V = 12 \sim 15$. Finally, HATNet and WASP projects monitor stars with apparent magnitude $V = 9 \sim 12$. These projects have detected many transit exoplanets, and the fraction of stars hosting a planet is consistent with the results suggested by Jiang et al. (2010). However, the brighter stars with $V < 5$ mag remain unexplored. It is not clear yet whether or not there are any exoplanets orbiting around these brighter stars. *In particular, when the brighter stars are nearby, it is very interesting to investigate whether there are any habitable exoplanets moving around them.*

BRITE (BRITe Target Explorer) is a space-based project with five operating nano-satellites that are equipped with telescopes of 3 cm aperture (Weiss et al. 2014). The main task of BRITE is to monitor bright stars, and the photometry precision is around mmag for stars brighter than $V \sim 5$ mag. It has studied oscillation modes of many pulsating stars. For example, BRITE photometry detected several new modes for the β Cep star HD29248 (Handler et al. 2017). This star now has ten low-order modes and seven high-order gravity modes. Potentially, BRITE could also pose some observational constraints on the number of exoplanets hosted by nearby bright stars. Passegger and Weiss (2006) estimated the number of exoplanet transits which could be detected by BRITE for the main sequence stars brighter than $V = 4$ mag. They concluded that a few Neptune-sized and Jupiter-sized exoplanets shall be detectable. Mol Lous et al. (2018) was the first to search for transiting planets in β Pictoris system from the BRITE data because this system was well monitored by BRITE and might detect additional planets given that a Jupiter-mass planet, β Pictoris b, was directly imaged in 2009 (Lagrange et al. 2009, 2010). Although Mol Lous et al. (2018) did not report a positive result, this gave us the impetus to examine the BRITE data through a new transit searching method such as the machine-learning technique.

The conventional method used for the transit detection task is to calculate some important quantities from the data, and then criteria are set to automatically classify them. For complicated cases, one might need to make several levels of judgment and build up a pipeline to deal with the data. The main advantage of machine learning is that the computer code gets modified and can be improved by itself through a learning process. The conditions of

classification can be changed, thus, improving the capability of making correct judgments.

Machine learning has been employed to investigate many astronomical problems in recent years (Longo et al. 2019). It was used to classify the morphology of galaxies (Perez-Carrasco et al. 2019) and the spectrum of stellar objects (Passegger et al. 2020) and to model stellar oscillation modes. In particular, Hendriks and Aerts (2019) employed a deep learning technique to carry out asteroseismic modeling of the β Cep star HD29248 and found it to be a rather evolved star.

In fact, machine learning is already in use as a new tool to vet or detect exoplanets. Pearson et al. (2018) showed a triage to employ machine learning to search for new exoplanet transits. They compared the results obtained through several methods. Likewise, Shallue & Vanderburg (2018) demonstrated that the machine learning technique, particularly the convolutional neural network (CNN), can be useful to vet and confirm threshold crossing events and lead to the discoveries of new exoplanets. Recently, Ansdell et al. (2018) suggested to include stellar parameters, etc. into CNN structures for improved accuracy. Later, Dattilo et al. (2019) employed CNNs to identify two previously unknown exoplanets from the K2 mission of the Kepler Space Telescope. Yu et al. (2019) attempted to use CNNs to vet possible transits from the newly released data of the Transiting Exoplanet Survey Satellite (TESS).

Considering the above-mentioned developments, in this study, we planned to employ the CNN of deep learning to examine whether there are exoplanet transit candidates in BRITe data. As BRITe mainly monitors bright stars, we expected to gain some statistical data about exoplanets around these bright stars, with an aim to improve our understanding of the general picture of the overall exoplanet population.

Machine learning and CNN are briefly summarized in §2. The observational BRITe data and the preparation of CNN input light curves are presented in §3. The training of our CNN models is described in §4, the results are presented in §5, followed by conclusions in §6.

2. Machine Learning with Convolutional Neural Network

In machine learning, when some data is given as an input to a computer code, the code does some calculations and produces results that are taken as a feedback to improve the computer code itself. Deep learning is a type of machine learning technique that imitates the human brain and consists of many calculation units called neurons. Several neurons are assigned to one layer. Usually, a number of layers are needed and they are connected to

form a neural network. When the input data of a layer is designed to do the convolution with a filter, i.e. kernel, this layer is called a convolutional layer. When a neural network consists of convolutional layers, it is called a CNN. An introduction of CNN can be found in Chintarungruangchai & Jiang (2019).

In this study, we have considered the one-dimension convolutional neural network (1D-CNN) of machine learning techniques. With this deep-learning technique, we decided to examine the possible transits with periods from one to five days. One way to proceed was to train a CNN model through synthetic light curves with the above transit periods and use this CNN model to detect possible transits from data. However, to make our CNN models more sensitive to the transit signals with specified periods, we decided to have four different CNN models that focus on different periods. Thus, there were

- (a) Model P12: the detection of possible transits with periods between one and two days;
- (b) Model P23: the detection of possible transits with periods between two and three days;
- (c) Model P34: the detection of possible transits with periods between three and four days;
- (d) Model P45: the detection of possible transits with periods between four and five days.

The architecture of the above 1D-CNN models contains four convolutional layers. For each convolutional layer, the channel number, kernel size, and stride were set as 64, 5, 1, respectively. In addition, when we trained Model P12, only those samples were employed which injected transit signals with periods between one and two days. Similarly, Model P23, Model P34, Model P45 were also trained by the light curves with corresponding transit periods.

3. The Light Curves

In this section, the BRITE observational light curves are described. In addition, the procedure to inject transit signals into light curves, and the details of light-curve folding are also presented.

3.1. BRITE Data

For this study, all BRITE data sets of Data Release 2 (R2) and Data Release 3 (R3) were retrieved from BRITE Public Data Archive. These data sets were obtained by five BRITE nano-satellites: blue-filter BRITE-Austria (BAb), red-filter BRITE-Heweliusz (BHR), blue-filter BRITE-Lem (BLb), red-filter BRITE-Toronto, and red-filter Uni-BRITE (UBr). The name of the monitored star, the observational duration, and the names of the employed nanosatellite name are clearly mentioned in the header of each data file. For one particular

star, there could be more than one data file. In this case, we would check which nano-satellite was used to obtain the measurements in these data files. If the observations were done by different nano-satellites, they were considered to be separate light curves. If the photometric measurements in several files were done through the same nano-satellite, these measurements were combined to become one light curve.

Our goal was to detect possible transit candidates from a large number of light curves, therefore, to be efficient, we planned to use a simple procedure to reduce the scattering of light curves without going through elaborate corrections (Popowicz et al. 2017). Thus, we chose suitable intervals to bin the data to average out the scattering. We decided to calculate the average flux within a 20-minute bin. This choice of 20 minutes can maximize the scattering reduction but still would have several data points for one transit event because a typical transit duration is about 60 to 200 minutes. The above-binned data was normalized with respect to the averages of observational runs. Then, the standard deviation was determined and the 3σ outlier data was removed. All light curves were obtained in this study through the above procedure before any further analysis. They were referred to as BRITE *light curve* hereafter. Fig. 1 shows one such BRITE light curve of the star HD37468 as an example. All the BRITE data sets used in this study are listed in Table 1. In total, there are 35 BRITE light curves.

3.2. Injecting Transit Signals

To search for transit candidates from light curves, the CNN model needs to be trained by both non-transit and transit light curves. The BRITE light curves were used as the training samples of non-transit light curves. The transit signals were injected into the BRITE light curves to produce synthetic transit light curves to be used as training samples.

However, there may be real transits in BRITE light curves, and thus they cannot be used as non-transit training samples. As presented in the next subsection, the BRITE light curves were folded with a huge number of assumed trial periods. For almost all cases, the possible real transit signals were destroyed during the folding process. The probability that the real transit is not destroyed in folded light curves is extremely small. A huge number of training samples were employed, this tiny defect did not affect the training results of CNN models. Thus, the folded BRITE light curves were treated as non-transit light curves in training samples.

The transit signals were modeled by the method in Mandel and Agol (2002). The parameters included the transit period (p), the ratio of the orbital semi-major axis to the

Satellite	Data ID	Star	Number of Data Points (N)	Standard Deviation (σ)
BAb	(BAb-1)	HD37043	1385	0.00444
	(BAb-2)	HD121263	1870	0.00388
	(BAb-3)	HD35468	1380	0.00279
	(BAb-4)	HD33111	1116	0.00435
BHr	(BHr-1)	HD37468	2022	0.00452
	(BHr-2)	HD35468	1995	0.0049
BLb	(BLb-1)	HD35468	1842	0.00377
	(BLb-2)	HD186882	1574	0.0039
BTr	(BTr-1)	HD80404	1397	0.00342
	(BTr-2)	HD34503	1382	0.00422
	(BTr-3)	HD79351	1387	0.00467
	(BTr-4)	HD198183	1569	0.00449
	(BTr-5)	HD74772	1399	0.00284
	(BTr-6)	HD82434	1406	0.00371
	(BTr-7)	HD81188	1388	0.00411
	(BTr-8)	HD74006	1396	0.00304
	(BTr-9)	HD64740	1400	0.00463
	(BTr-10)	HD33111	1380	0.00336
	(BTr-11)	HD68553	1391	0.00496
	(BTr-12)	HD30652	1370	0.00407
	(BTr-13)	HD202444	1224	0.00225
	(BTr-14)	HD35468	1378	0.00370
	(BTr-15)	HD76728	1375	0.00468
	(BTr-16)	HD64440	1399	0.00252
	(BTr-17)	HD78004	1374	0.00455
	(BTr-18)	HD71129	1395	0.00384
	(BTr-19)	HD36512	1380	0.00485
	(BTr-20)	HD74575	1082	0.00392
	(BTr-21)	HD186882	1222	0.00245
UBr	(UBr-1)	HD20902	3742	0.00440
	(UBr-2)	HD23630	3736	0.00478
	(UBr-3)	HD121263	2648	0.00426
	(UBr-4)	HD33111	1413	0.00395
	(UBr-5)	HD134505	2646	0.00491
	(UBr-6)	HD35468	1405	0.00468

Table 1: BRITE light curves

stellar radius (a_{rmos}), the ratio of planet radius to the stellar radius (R_{rmps}), the orbital inclination (i), the linear limb darkening coefficient (u_1), and the quadratic limb darkening coefficient (u_2). As described in the previous section with the four CNN models which correspond to different ranges of transit periods, the parameter p was set to be uniformly distributed between one and two days for Model P12, two and three days for Model P23, three and four days for Model P34, four and five days for Model P45. Other parameters are set to be uniformly distributed within the intervals shown in Table 2.

The transit light curves after injecting these transit signals into the BRITE data are presented as Fig. 2. For convenience, the transit period (p) was set at 1 day for the results in Fig. 2. Fig. 2(a)-(c) present the outcomes injecting the transit signal into the BRITE light curve of the star HD68553, and Fig. 2(d)-(f) present the outcomes for the star HD202444. From these plots, it is clear that the transit depth is much more sensitive to the parameter R_{ps} .

3.3. The Folding

BRITE is not designed for the detection of exoplanets, so the time for data resolution and monitoring duration is very different from usual transit observations. The main characteristics of BRITE data are the high time resolution within intervals of about 15 minutes and various gaps between these intervals. Thus, the folding is the best way to reveal the possible transit signals.

However, folding can enhance the signals when the folding period is the same as the signal period and can destroy signals when the folding period is different from the signal period. Therefore, we had to conduct folding for different trial periods, and a huge amount of folded light curves could be produced. The CNNs of machine learning then play a very important role in judging which ones are transit candidates.

To enable the CNN models to detect transits from those light curves folded with slightly

parameter	range
a_{os}	10-30
R_{ps}	0.06-0.15
i	86-90 (degrees)
u_1	0.5
u_2	0.0

Table 2: Parameters of transit signals

different periods, we also carried out folding with periods that were two-minute shorter and two-minute longer than the transit period, i.e. $p \pm 2/1440$ (day). In Fig. 3, we present both transit light curves and non-transit light curves of two stars after folding. The folding periods for the star HD68553 in Fig. 3(a)-(c) were set to be 1438 minutes, 1440 minutes, and 1442 minutes, respectively. Similarly, the folding periods for the star HD202444 in Fig. 3(d)-(f) were set to be 1438 minutes, 1440 minutes, and 1442 minutes, respectively. Other transit parameters include $a_{\text{os}} = 20.0$, $R_{\text{ps}} = 0.07$, $i = 88$, and period $p = 1(\text{day}) = 1440(\text{min})$ for all light curves in Fig. 3.

4. The Training Processes

For a given number of light curves N_t (which is usually larger than 10000), 80% of these are used as the training data, 10% include the validation data, and the remaining 10% are the testing data. Note that half of all the above light curves are transit light curves and half are non-transit light curves. The training data was separated into subsets, called mini-batches. We randomly assigned 16 light curves to each mini-batch (except the final mini-batch which had fewer light curves). Each mini-batch was fed into the CNN model one by one until all were used. When all training data are used, it is called one epoch. Before the next epoch starts, the light curves in mini-batches are randomly assigned again. We observed many epochs, and every time right after one epoch was completed, the CNN model was used to predict the answers of the validation data. The percentage of the correct answers was defined to be “accuracy”, and each epoch had a value of accuracy. The stopping condition of the training process was indicated when the difference of two successive accuracies was less than 0.001 and the number of epochs was larger than 25. Once the training process stopped, the CNN model settled and could be used to predict the answers of the testing data and obtain the corresponding accuracy.

4.1. The CNN Models

Here we describe how we obtained the CNN models, i.e. Model P12, P23, P34, and P45, which were used to search for possible transits. Taking Model P12 as an example, we first needed to inject transit signals into BRITE light curves. To decide a transit signal to be injected, we chose a period p through a uniformly distributed random number ranging between one and two days. Concurrently, other parameters a_{os} , R_{ps} , and i were also randomly chosen from uniform distributions within the intervals listed in Table 2.

Each light curve was folded with the same chosen period p . When p is between one day and two days, the number of data points of one light curve is between 72 and 144 (because the bin size was set as 20 min). To make the Model P12 always have the same number of input nodes, we used interpolation to generate 144 data points for all light curves and set the number of input nodes as 144 for Model P12. Each light curve was also folded with a period that is two-minute larger and two-minute smaller than p . Thus, three folded light curves were generated from one BRITE light curve. These three were injected with the chosen transit signal and generated another three folded light curves with transit. Therefore, a total of six folded light curves were generated from one BRITE light curve to become a standard input with 144 nodes for Model P12.

The typical number of training samples is usually larger than 10000 for the construction of any CNN models (Pearson et al 2018). Thus, we used a random number to decide which BRITE light curves could be used to generate six folded light curves. All our 35 BRITE light curves were candidates to be picked and this is repeated until there are several N_s input light curves ($N_s=6000$).

Each of these generated input light curves was used as training samples following the process previously described. The whole process was repeated five times to get five Model P12. Other CNN models, such as Model P23, Model P34, and Model P45 were also produced in the same way. In Table 3, the range of periods, input node numbers, and the accuracies are listed. Besides the accuracy, the results of reliability (the percentage of real transit light curves among those light curves which predicted to have transits) and completeness (the percentage of the light curves that are successfully predicted to have transits among those transit light curves) are also presented in Table 3. Because all CNN models were trained five times, five versions of Model P12, Model P23, Model P34, Model P45 could be generated. The values of accuracy, reliability, and completeness represent the corresponding median values, and the errors are their standard deviations of five versions. All five versions of these CNN models were employed to search for possible transits.

Model	period (day)	Input Node Number	accuracy (%)	reliability (%)	completeness (%)
P12	$p = 1 \sim 2$	144	99.76 ± 0.069	99.81 ± 0.195	99.68 ± 0.077
P23	$p = 2 \sim 3$	216	99.90 ± 0.030	99.94 ± 0.079	99.95 ± 0.042
P34	$p = 3 \sim 4$	288	99.85 ± 0.026	99.78 ± 0.093	99.90 ± 0.048
P45	$p = 4 \sim 5$	360	99.78 ± 0.033	99.99 ± 0.056	99.63 ± 0.093

Table 3: CNN models

4.2. The Learning Curve

The accuracy of a CNN model is proportional to the sample size but it may get saturated when the sample size is big enough. Thus, to determine the best sample size, it is important to produce the learning curve, i.e. the accuracy of a CNN model as a function of sample size. With $N_s = 6000$, six different total numbers of light curves, $N_t = 2N_s, 4N_s, 8N_s, 16N_s, 32N_s$, and $64N_s$, were used to train Model P12 to obtain the learning curve here.

For each sample size N_t , five cycles of training, validation, and testing were done with different sample sizes. Finally, five accuracies were obtained. The median value is defined as the accuracy of a particular N_t , and the standard deviation gives the error bar. The accuracy as a function of N_t , i.e. the learning curve, is presented in Fig. 4. From Fig. 4, we observe that the accuracy is stable when the sample size is $N_t = 32N_s$, so the total number of employed light curves is $N_t = 32N_s$, where $N_s = 6000$, for the construction of CNN models.

5. The Results

The results of the detection of transit candidates through CNN models are described here. We found a number of transit candidates and discuss two most likely transits that were modeled.

5.1. Transit Detection

After five versions of Model P12 were obtained, they were used to search for possible transits with periods between one and two days from our 35 BRITE light curves. To be ready as an input of Model P12, each BRITE light curve was folded with a folding period $fp = 1440 + j$ minute, where $j = 0, 2, 4, 6, 8, \dots, 1440$. Only those detected by all five versions of Model P12 were considered as the transit candidates here. Then, Model P23, Model P34, and Model P45 were employed to search for possible transits with larger periods in the same way.

The folding periods, in minutes of all the transit candidates detected by our CNN models, are listed in Table 4. The first column of Table 4 represents the Data ID of BRITE light curves originally assigned in Table 1. The second column is the transit period detected by Model P12. The third, 4th, and 5th columns are the transit periods detected by Model P23, Model P34, and Model P45, respectively. For example, for light curve BAb-1, three transits were detected. They represent transits with periods of 2160 minutes, 2892 minutes,

and 6338 minutes. These three transits are put in different rows as they correspond to different periods. For light curve BAb-4, only one transit was detected. However, many more transits were detected for the light curve BHr-1. In particular, the transit with a period of 1714 minutes was detected repeatedly by three CNN models, Model P12, Model P23, and Model P34. In addition, for the light curve BLb-2, the transit with a period of 1440 min was also detected by more than one CNN models. Therefore, among all detected transit candidates, these two have larger probabilities to be real transits. However, one must be cautioned that 1440 min is exactly one day. Though BRITE is a space instrument, it might still suffer from various issues related to stability. Therefore, the transit for 1440 min could be a false one. The confirmation is out of the scope of this paper and is left for future further studies. The other transit candidates were only detected, possibly due to weak signals, by one CNN model and we decided to leave them to be investigated when there are more high-precision data available in the future.

5.2. HD37468 and HD186882

Let us discuss these two systems whose light curves exhibit real detected transits here. The star HD37468, which gives light curve BHr-1, is also named as σ Ori. It is actually a system with several stars. Among these stars, σ Ori A and σ Ori B form a visual binary with an orbital period of about 160 years. In addition, σ Ori A is a binary star itself, comprising σ Ori Aa and σ Ori Ab, and their orbital period is 143 days. The detected 1714 min photometrical variation is definitely not due to the orbital motion of the binary σ Ori Aa and σ Ori Ab.

These three stars appear very close to each other (within 0.26 arcsec) in the sky, and are not resolved by the BRITE telescope. Considering the stability, there may be a certain level of mass difference between three stars, which must be the most massive one which dominates the observed flux. It is likely that the 1714 min periodical variation could be due to an exoplanet orbiting around the most massive star.

Though the system seems to be complicated, the photometric transit parameters could still be obtained as an estimation, assuming that the most massive star dominates the observed flux and the planet is moving around the most massive one. Here the model in Mandel & Agol (2002) is employed to fit the observational light curve through a Markov-Chain Monte-Carlo (MCMC) sampling process. Note that the limb-darkening effect is ignored for the occultation part of the light-curve model. The orbital period was fixed at 1714 minutes, the inclination was fixed to $i = 90$, the limb-darkening coefficients were fixed to the values mentioned in Table 2. Other five parameters, including the mid-transit time (t_{tra}), the mid-

Data ID	Model P12	Model P23	Model P34	Model P45
(BAb-1)	2160			
		2892		
				6338
(BAb-4)			5704	
(BHR-1)	1714	1714×2	1714×3	
	1716			
		4220		
			5144	
			5146	
(BLb-1)	1456			
(BLb-2)	1440		1440×3	
	1444			
	2868			
	2870			
	2872			
	2876			
	2878			
		4312		
		4314		
		4316		
		4318		
			4324	
				5772
				7188
				7196
(BTr-2)			4324	
(BTr-12)			4624	
				6986
				7174
(BTr-15)			5014	
(BTr-19)		4230		
			4324	
			4722	
(BTr-20)	2656			
(UBr-5)	2870			
	2872			

Table 4: The detected transit candidates

occultation time (t_{occ}), the ratio of the orbital semi-major axis to the stellar radius (a_{os}), the ratio of planetary radius to the stellar radius (R_{ps}), and the ratio of planetary flux to stellar flux (f_{ps}) were treated as MCMC samples.

The MCMC sampling code *MC3*, provided by Cubillos et al. (2017), was used to generate seven chains of 10^5 samples. The best-fit model is then obtained with a value of reduced chi-square $\chi_{\text{red}}^2 = 2.39$. In Fig. 5, the observational data is shown as points and the best-fit model is presented as the solid line. Fig. 6 presents the two-dimensional and one-dimensional projections of MCMC posterior distributions, where the dashed lines indicate the best-fit model.

The star HD186882, which gives light curve BLb-2, is also named as δ Cyg. It is a binary system with components δ Cyg A and δ Cyg B. Their separation is about 157 AU and they orbit around each other with a period 780 years. In the sky, their angular separation is about 3 arcsec, thus they cannot be resolved by the BRITE telescope. Their combined apparent magnitude was observed to be nearly 2.87. The primary star δ Cyg A is much brighter than the companion star δ Cyg B. The detected transit with a period of 1440 min could be due to a close-in exoplanet or a sub-stellar object orbiting around δ Cyg A.

The photometric transit parameters could be obtained similarly as described above. As there is no occultation part for the light curve here, with a fixed orbital period of 1440 min, fixed inclination, and fixed limb-darkening coefficients as before, only three parameters, t_{tra} , a_{os} , R_{ps} , are needed for the transit model. Using the same MCMC sampling process, the best-fit model was then obtained with a value of reduced chi-square $\chi_{\text{red}}^2 = 4.10$. The best-fit model and the observational light curve are shown in Fig. 7. The MCMC posterior distributions of these three transit parameters are presented in Fig. 8.

6. Concluding Remarks

To explore the possible existence of exoplanets around brighter stars, we searched for exoplanet transits from photometrical data obtained by the BRITE satellite through a machine learning technique. Considering exoplanets with orbital periods from one to five days, four CNN models focusing on different periods were constructed. They were trained with synthetic data generated by injecting planetary transit signals into the BRITE light curves.

Using these four CNN models, i.e. Model P12, P23, P34, and P45, to examine the BRITE light curves of 35 stars, 10 stars exhibited possible transits detected by at least one CNN models, but only two of them were detected by more than one CNN model. These two have larger probabilities to be true planetary transits. Their transit parameters were further

estimated through an MCMC sampling, and the results show that they could be close-in Jupiter-mass exoplanets. The future high-precision observational data will be very useful in clarifying whether there are exoplanets in these 10 candidates and also lead to a much better determination on the orbital parameters. While this study demonstrated that our CNN models could successfully identify possible transit candidates, we caution that further investigation with additional observational data is necessary to lead to final confirmations.

Acknowledgments

We are thankful to the referee for very helpful suggestions. This work is based on data collected by the BRITe Constellation satellite mission, designed, built, launched, operated and supported by the Austrian Research Promotion Agency (FFG), the University of Vienna, the Technical University of Graz, the Canadian Space Agency (CSA), the University of Toronto Institute for Aerospace Studies (UTIAS), the Foundation for Polish Science & Technology (FNiTP MNiSW), and National Science Centre (NCN). This project is supported in part by the Ministry of Science and Technology, Taiwan, under Li-Chin Yeh’s Grant MOST 106-2115-M-007-014 and Ing-Guey Jiang’s Grant MOST 106-2112-M-007-006-MY3.

REFERENCES

- Ansdell, M., Ioannou, Y., Osborn, H. P. et al. 2018, *ApJL*, 869, L7
- Borucki, W. J., Koch, D. G., Basri, G. et al. 2011, *ApJ*, 736, 19
- Chintarungruangchai, P., Jiang, I.-G. 2019, *PASP*, 131, 064502
- Cubillos, P., Harrington, J., Lored, T. et al. 2017, *AJ*, 153, 3
- Dattilo, A., Vanderburg, A., Shallue, C. J. et al. 2019, *AJ*, 157, 169
- Handler, G., Rybicka, M., Popowicz, A. et al. 2017, *MNRAS*, 464, 2249
- Hendriks, L., Aerts, C. 2019, *PASP*, 131, 108001
- Ioannidis, P., Schmitt, J. H. M. M., Avdellidou, Ch., von Essen, C., Agol, E. 2014, *A&A*, 564, A33
- Jiang, I.-G., Yeh, L.-C., Chang, Y.-C., Hung, W.-L. 2010, *ApJS*, 186, 48
- Lagrange, A.-M., Bonnefoy, M., Chauvin, G. et al. 2010, *Science*, 329, 57

- Lagrange, A.-M., Gratadour, D., Chauvin, G. et al. 2009, *A&A*, 493, L21
- Longo, G., Merenyi, E., Tino, P. 2019, *PASP*, 131, 100101
- Mandel, K., Agol, E. 2002, *ApJ*, 580, L171
- Mol Lous, M., Weenk, E., Kenworthy, M. A., Zwintz, K., Kuschnig, R. 2018, *A&A*, 615, A145
- Passegger, V. M., Bello-Garcia, A., Ordieres-Mere, J. et al. 2020, *A&A*, 642, A22
- Passegger, V. M., Weiss, W. W. 2006, *Astron. Nachr.*, 999, 789
- Pearson, K. A., Palafox, L., Griffith, C. A. 2018, *MNRAS*, 474, 478
- Perez-Carrasco, M., Cabrera-Vives, G., Martinez-Marin, M., Cerulo, P., Demarco, R., Protopapas, P., Godoy, J., Huertas-Company, M. 2019, *PASP*, 131, 108002
- Popowicz, A., Pigulski, A., Bernacki, K. et al. 2017, *A&A*, 605, A26
- Shallue, C. J., Vanderburg, A. 2018, *AJ*, 155, 94
- Socia, Q. J., Welsh, W. F., Orosz, J. A. et al. 2020, *AJ*, 159, 94
- Sun, L., Ioannidis, P., Gu, S., Schmitt, J. H. M. M., Wang, X., Kouwenhoven, M. B. N. 2019, *A&A*, 624, A15
- Weiss, W. W., Rucinski, S. M., Moffat, A. F. J. et al. 2014, *PASP*, 126, 573
- Xie, J.-W. 2013, *ApJS*, 208, 22
- Yu, L., Vanderburg, A., Huang, C. et al. 2019, *AJ*, 158, 25

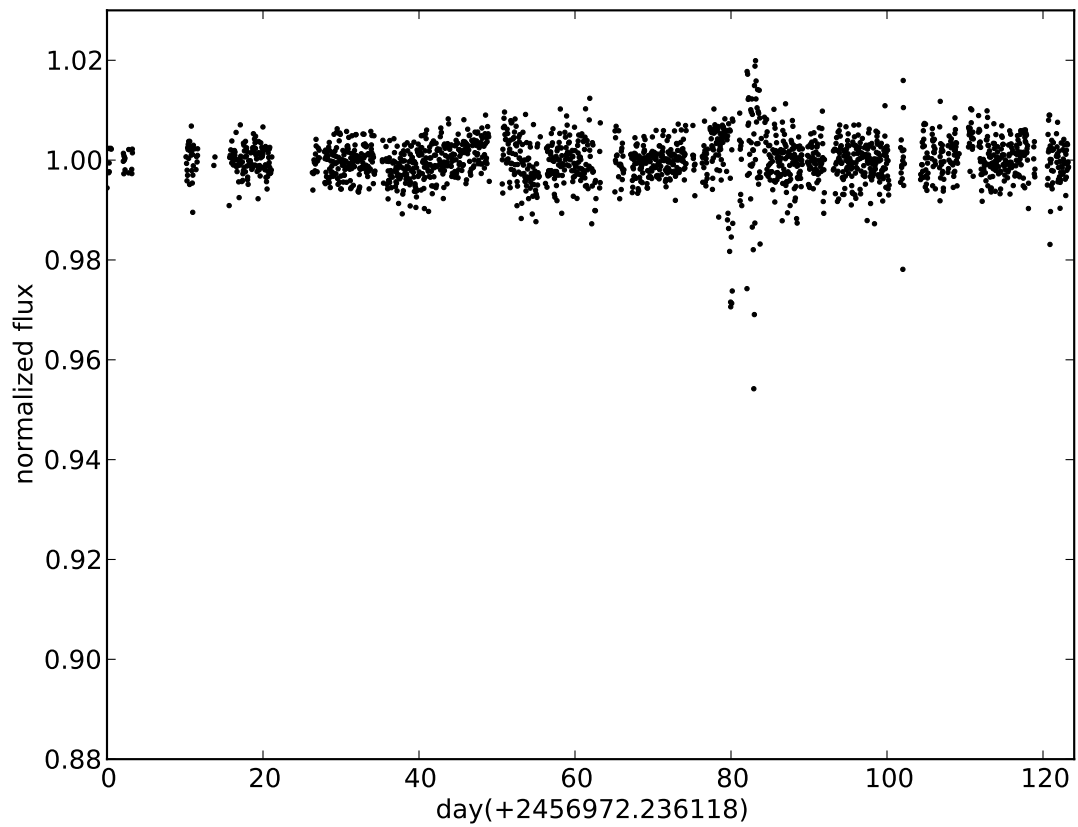


Fig. 1.— The BRITE light curve of HD37468.

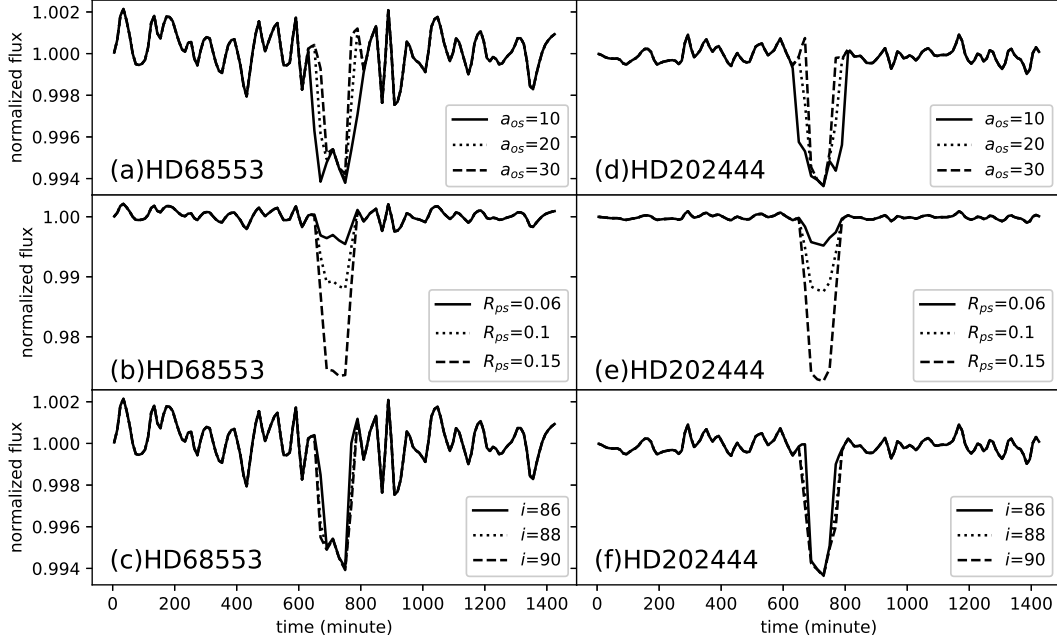


Fig. 2.— The synthetic light curves. The left panels represent the star HD68553, and the right panels represent the star HD202444. For top panels, $R_{ps} = 0.07$, $i = 88$, and $a_{os}=10$ (solid curves), 20 (dotted curves), 30 (dashed curves). For middle panels, $a_{os} = 20$, $i = 88$, and $R_{ps}=0.06$ (solid curves), 0.10 (dotted curves), 0.15 (dashed curves). For bottom panels, $a_{os} = 20$, $R_{ps} = 0.07$, and $i=86$ (solid curves), 88 (dotted curves), 90 (dashed curves).

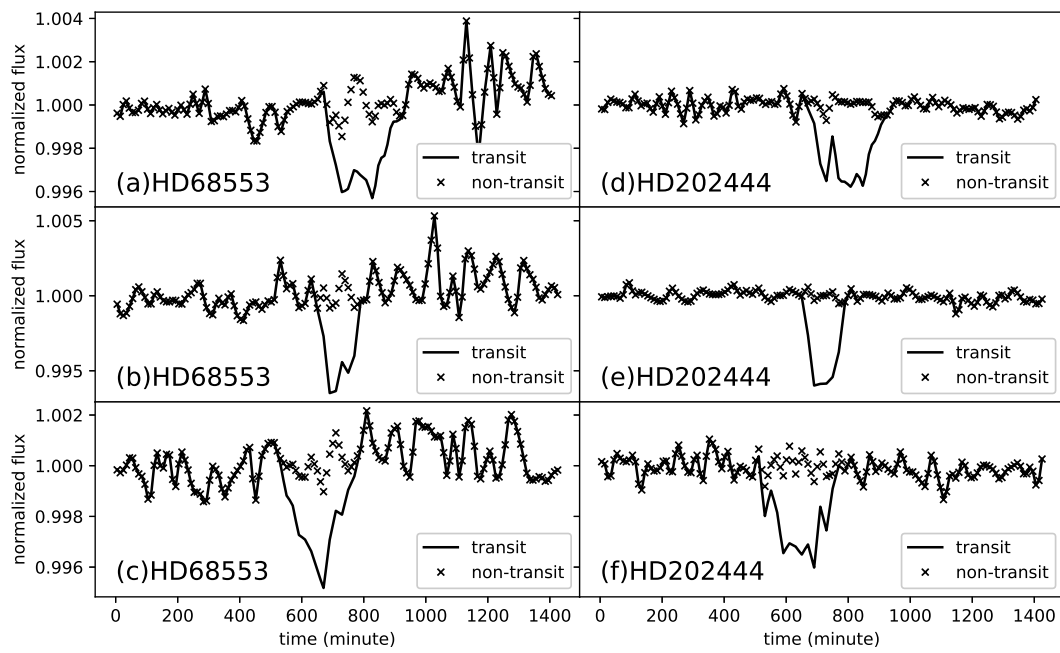


Fig. 3.— The folded light curves, where the solid curves are those with transit and the crosses are those without transit. The left panels represent the star HD68553, and the right panels represent the star HD202444. The folding periods for top panels, middle panels, and bottom panels are 1438 min, 1440 min, and 1442 min, respectively.

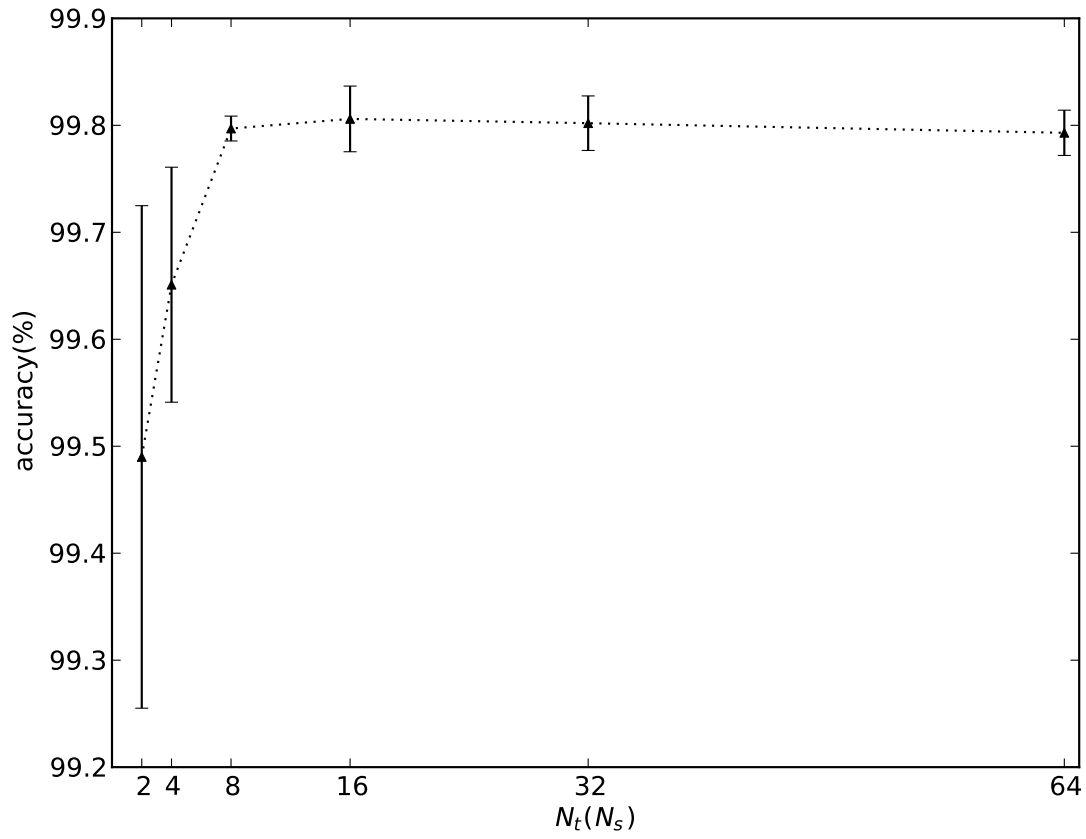


Fig. 4.— The learning curve, representing the accuracy as a function of training sample size.

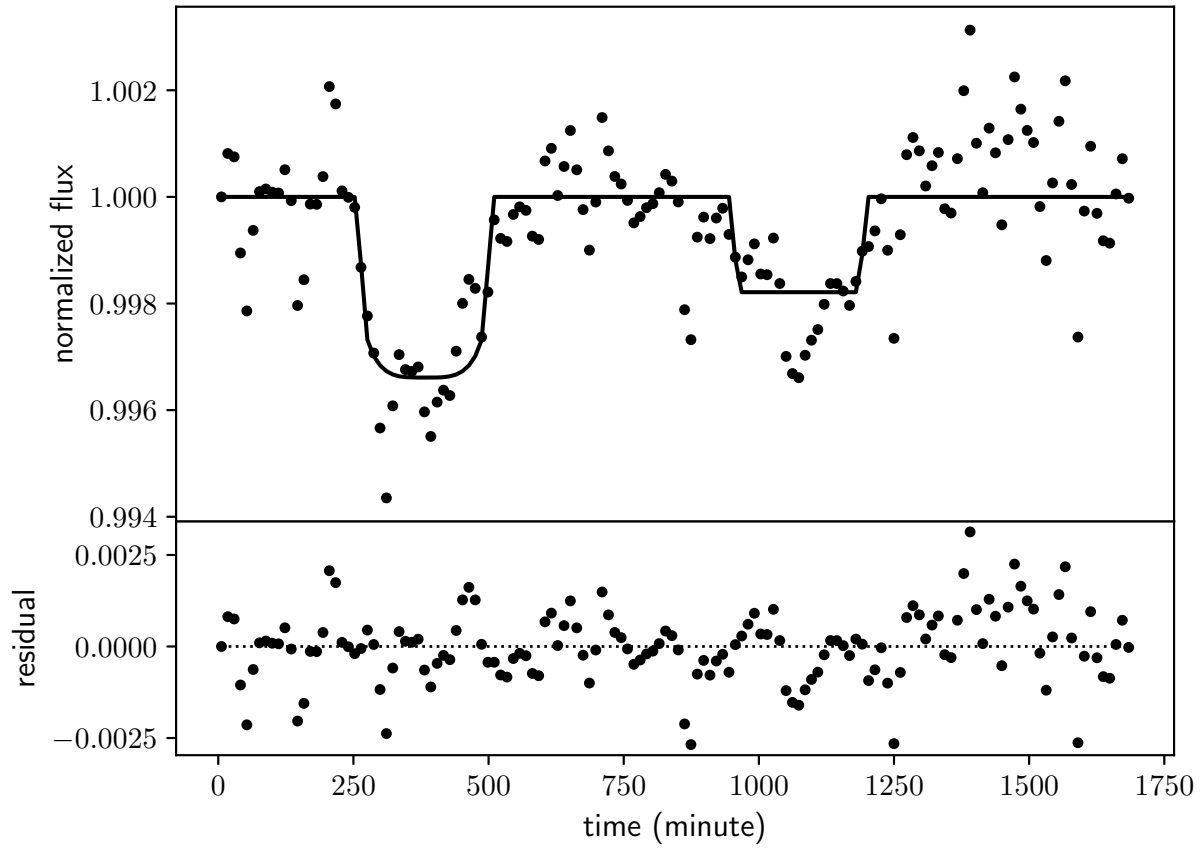


Fig. 5.— The folded BHR-1 light curve of the star HD37468. The points are the observational data with the folding period of 1714 minutes. The solid line represents the best-fit model.

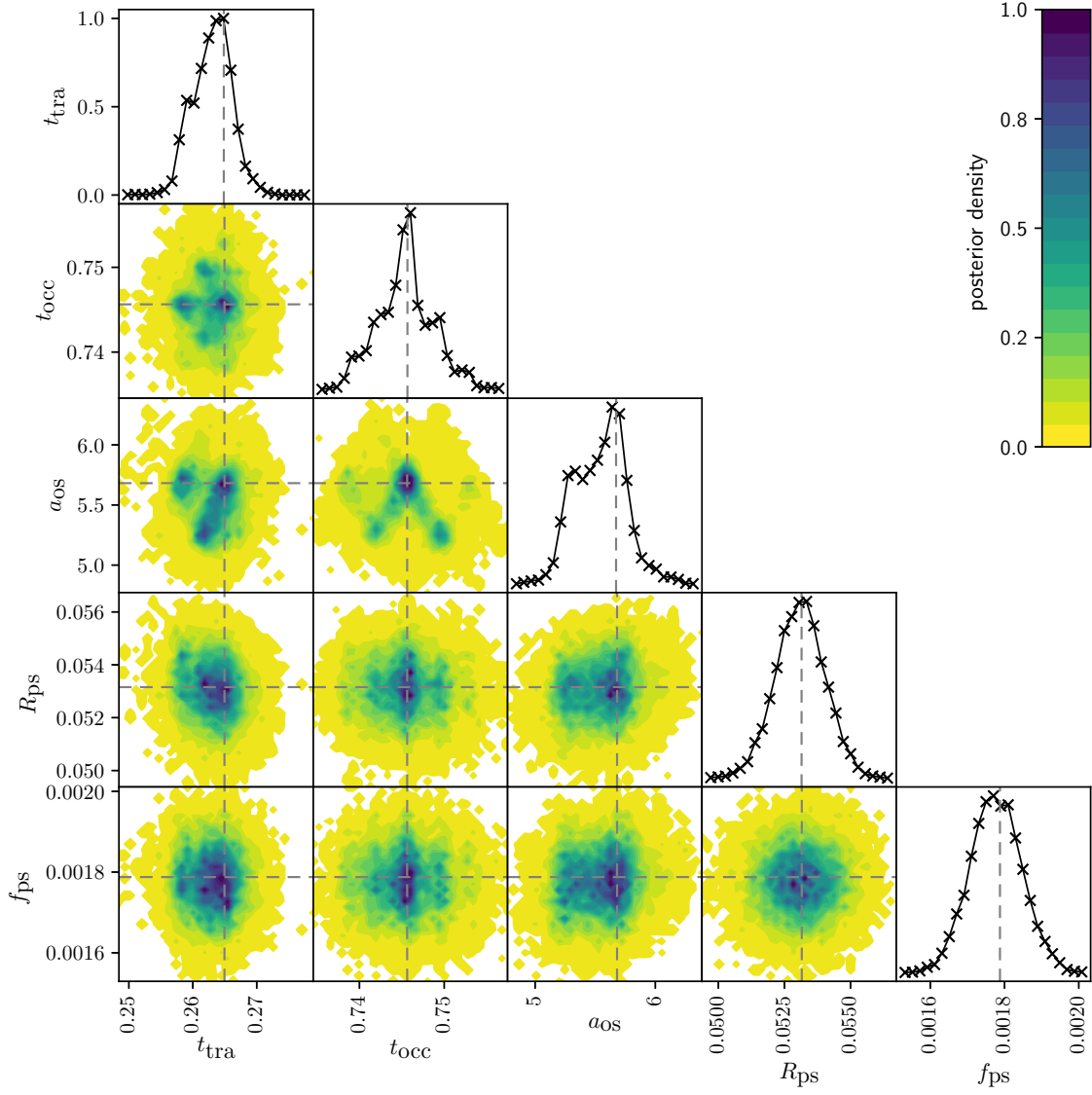


Fig. 6.— The MCMC posterior parameter distributions of BHr-1 light-curve modeling of the star HD37468. Those panels with colors are pairwise two-dimensional projections. The one-dimensional projections are presented as the histograms on the top. The dashed lines indicate the parameter values of the best-fit model.

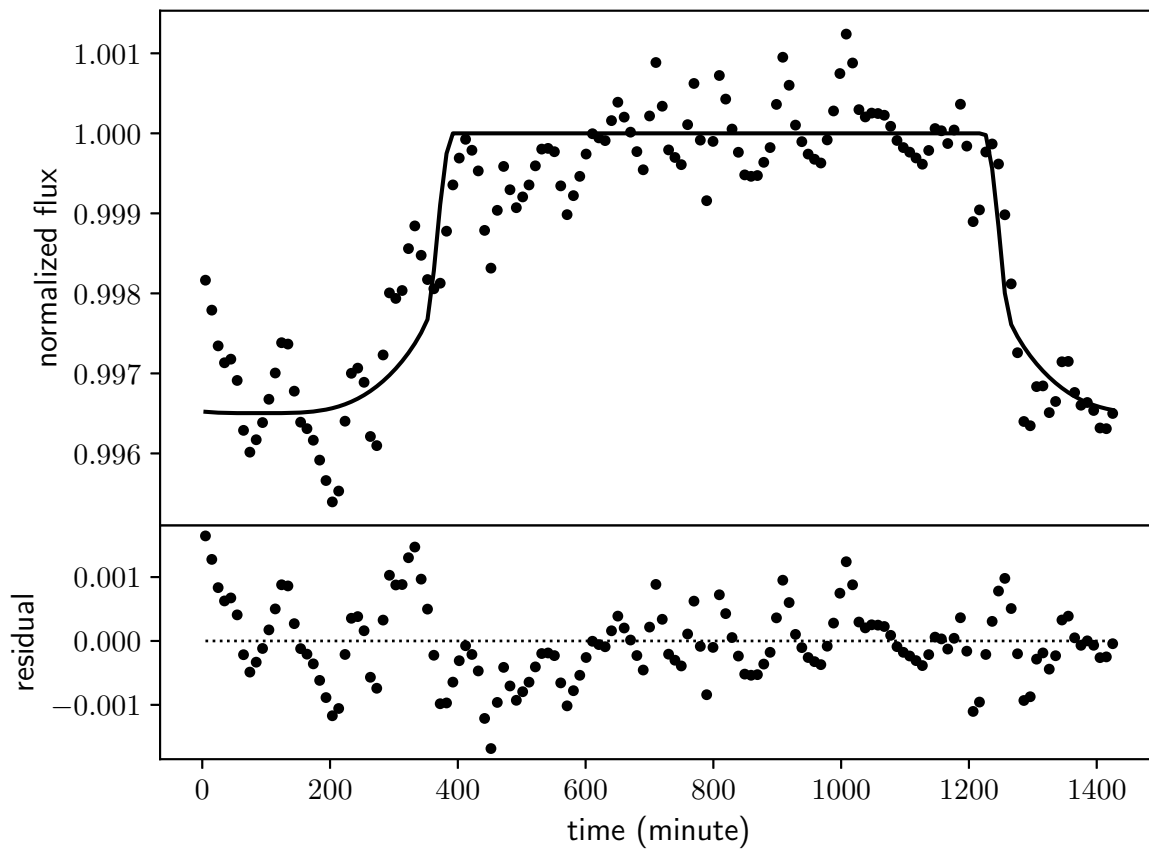


Fig. 7.— The folded BLb-2 light curve of the star HD186882. The points are the observational data with the folding period of 1440 minutes. The solid line represents the best-fit model.

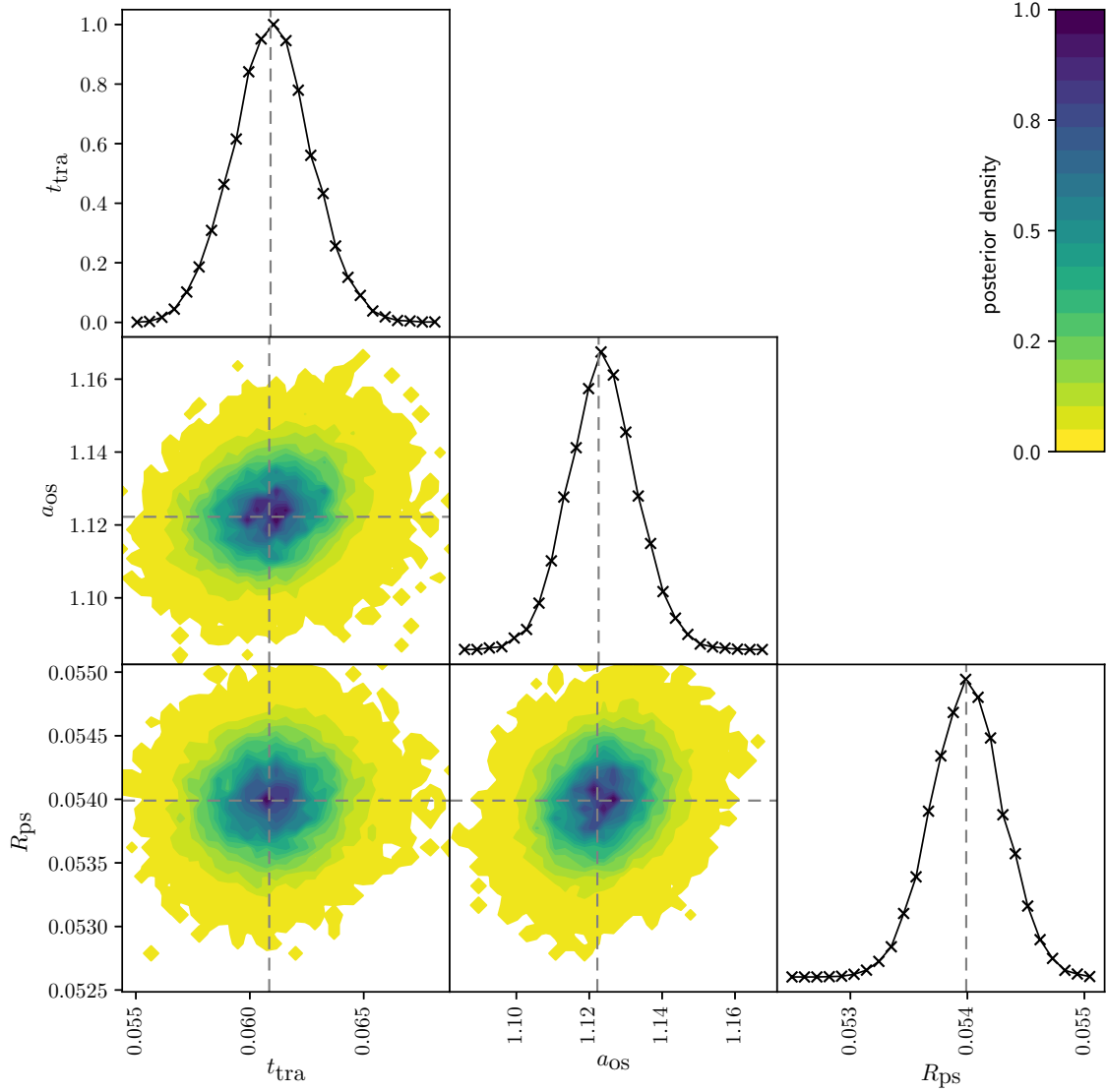


Fig. 8.— The MCMC posterior parameter distributions of BLb-2 light-curve modeling of the star HD186882. Those panels with colors are pairwise two-dimensional projections. The one-dimensional projections are presented as the histograms on the top. The dashed lines indicate the parameter values of the best-fit model.